Atmospheric Environment 341 (2025) 120888

Contents lists available at ScienceDirect

Atmospheric Environment

journal homepage: www.elsevier.com/locate/atmosenv

Aerosol retrievals derived from a low-cost Calitoo sun-photometer taken on board a research vessel

Rosa D. García [a,b], África Barreto [b,c,*], Celia Rey [b], Eugenio Fraile-Nuez [d], Alba González-Vega [d], Sergio F. León-Luis [a,b], Antonio Alcantara [b], A. Fernando Almansa [e,b], Carmen Guirado-Fuentes [b,c,f], Pablo González-Sicilia [b], Victoria E. Cachorro [c], Frederic Bouchar [g]

[a] TRAGSATEC, Madrid, 28006, Spain
[b] Izaña Atmospheric Research Center (IARC), State Meteorological Agency (AEMET), Santa Cruz de Tenerife, 38001, Spain
[c] Atmospheric Optics Group of Valladolid University (GOA–UVa), Valladolid, 47011, Spain
[d] Centro Oceanográfico de Canarias. Instituto Español de Oceanografía. Consejo Superior de Investigaciones Científicas (IEO-CSIC), Santa Cruz de Tenerife, 38001, Spain
[e] Cimel Electronique, Paris, 75011, France
[f] Now, Servicio de Evaluación del Servicio Canario de la Salud, Canary Islands, Santa Cruz de Tenerife, 38109, Spain
[g] TENUM, Toulousse, 31200, France

HIGHLIGHTS

- The 5-year Calitoo measurements strongly correlate with the AERONET-Cimel data, demonstrating their reliability for AOD observations.
- Calitoo has demonstrated remarkable calibration stability with an estimated AOD uncertainty of 0.032 ± 0.008.
- A reliable aerosol classification has been conducted using Calitoo AOD and AE data, which could significantly enhance our understanding of aerosols in remote or under-monitored areas.
- Calitoo measurements are representative over large scales in the subtropical region, particularly under marine clean and dusty conditions, highlighting its utility for aerosol monitoring.
- The low-cost Calitoo instrument can be a valuable tool for future research, helping to reduce current data gaps in global monitoring networks.

GRAPHICAL ABSTRACT

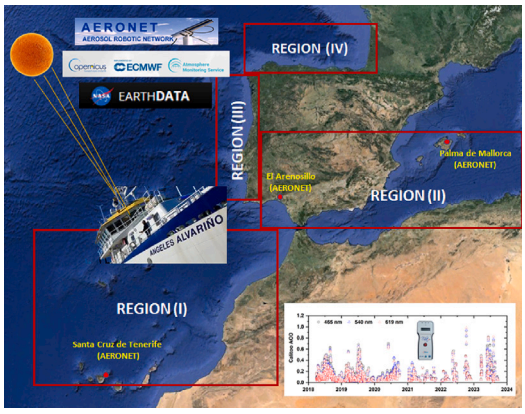

ARTICLE INFO

Dataset link: https://aeronet.gsfc.nasa.gov/, (https://ladsweb.nascom.nasa.gov), https://ads.atmosphere.copernicus.eu/

Keywords:
Aerosol optical depth

ABSTRACT

This study presents a comprehensive 5-year period assessment of aerosol optical depth (AOD) and Ångström Exponent (AE) data from a hand-held Calitoo sun photometer on board the *Ángeles Alvariño* research vessel. Observations spanned March 2018 to September 2023, focusing on key maritime regions such as the Canary Islands, coasts of North Africa, the Mediterranean, Portugal, the Cantabrian, and the Bay of Biscay. The Calitoo device measures solar irradiance at three wavelengths (465, 540, and 619 nm). Uncertainty analysis for Calitoo

* Corresponding author at: Izaña Atmospheric Research Center (IARC), State Meteorological Agency (AEMET), Santa Cruz de Tenerife, 38001, Spain.
E-mail address: abarretov@aemet.es (Á. Barreto).

https://doi.org/10.1016/j.atmosenv.2024.120888
Received 15 July 2024; Received in revised form 18 October 2024; Accepted 21 October 2024
Available online 12 November 2024

Calitoo sunphotometer
AERONET-cimel
MODIS
CAMS

AOD retrievals was performed using the Monte Carlo method, yielding an expanded uncertainty (U_{AOD}) ranging between 0.008 and 0.050 with a mean and standard deviation of 0.032 ± 0.008 for the three wavelengths. Our results also highlight the remarkable calibration stability of the Calitoo (< 2.6%) over this 5-year period. Calitoo AOD values were assessed using reference AOD data from Santa Cruz de Tenerife (the Canary Islands), El Arenosillo (Huelva), and Palma de Mallorca (the Balearic Islands) AERONET (Aerosol Robotic Network) stations. The comparison revealed a good agreement with correlation coefficients ranging from 0.727 to 0.917 and mean bias ranging from -0.030 to -0.001. Additionally, the Calitoo AOD data were compared with MODIS (Moderate Resolution Imaging Spectroradiometer) and CAMS-ECMWF (Copernicus Atmosphere Monitoring Service-European Centre for Medium-Range Weather Forecasts) aerosol products obtaining that Calitoo AOD values were generally lower, showing negative mean bias of -0.063 and -0.024, respectively.

The aerosol characterizations using AE vs. AOD plots in the three maritime study regions using 5-years of non-routine Calitoo data are similar to the corresponding aerosol characterizations performed with simultaneous AERONET-Cimel data.

These findings underscore Calitoo's reliability for aerosol studies in regions where AERONET instruments or other aerosol networks are unavailable. Likewise, given the low cost of Calitoo photometers, they could be deployed onboard a large number of merchant and passenger ships or in other remote or under-monitored areas, providing near real-time AOD/AE data to enhance our understanding of aerosols processes or for model or satellite assimilation/validation.

1. Introduction

Atmospheric aerosols play a crucial role in shaping the dynamics of global climate and air quality through intricate interactions with radiation and clouds. Their concentration, and consequently their radiative impact, exhibit significant heterogeneity across space and time, instigating climate variations at local, regional, and hemispheric scales (Garnés-Morales et al., 2023; Li et al., 2022). Emerging clean air regulations project a swift evolution in anthropogenic aerosol emissions in the upcoming decades, contributing to strong, spatially intricate trends and triggering extreme events not only near emission sources but also at distant regions (Persad et al., 2023). According to the sixth Assessment Report (AR6) of the Intergovernmental Panel on Climate Change (IPCC) (Forster et al., 2021) and, despite the increased understanding of aerosol-cloud interactions made in this report, the uncertainty in the effective radiative forcing of aerosols (ERF_{aer}) represents one of the largest uncertainties in our quantification of global climate change.

While field experiments provide the most comprehensive analysis of the aerosol radiative impact, they offer limited temporal and spatial information on aerosol properties (Smirnov et al., 2002). Satellite remote sensing can provide global, long-term information on atmospheric aerosols, although it is subjected to significant uncertainties due to radiometric calibration, required assumptions on aerosol properties, cloud contamination, or issues related to surface reflectivity (Li et al., 2009). Remote sensing through ground-based observations allows us to monitor aerosol micro-physical and optical properties with excellent spatial and temporal coverage (Holben et al., 2001; Smirnov et al., 2002; Torres et al., 2017; Cuevas et al., 2019, and among others). The AErosol RObotic NEtwork (AERONET; https://aeronet.gsfc.nasa.gov/) (Holben et al., 1998; Giles et al., 2019), the Sky Radiometer Network (SKYNET; https://www.skynet-isdc.org) (Kobayashi and Shiobara, 2015; Nakajima et al., 2020), and the Global Atmosphere Watch-Precision Filter Radiometer (GAW-PFR; https://www.pmodwrc.ch/weltstrahlungszentrum/worcc/gaw-pfr-network/) (Wehrli, 2000, 2005) are the most important monitoring networks due to their extensive coverage and high standardization levels.

Low-cost sensors are considered a key emerging technology for increasing monitoring density, with the capability of providing near-real-time and multi-pollutant spatially distributed information. Their use could significantly impact source identification and attribution, health and environmental justice applications, and forecast evaluation (Peltier et al., 2021) (Mailings et al. 2024). These sensors have been proven to provide a good quantification of local source impacts, such as those within the urban-sized network concept (Toledo et al., 2018). Their portability and compact size make them ideal for use in mobile monitoring studies tracking high pollution events, providing valuable insights into aerosol contributions near industrial areas or hotspots such as wildfires, and even estimating the reduction in aerosol impact due to COVID-19 related lockdowns (Giordano et al., 2021, & references therein).

However, as reported in Mailings et al. (2024) and references therein, careful evaluation of their outcomes through transparent reports is needed, using appropriate validation strategies and metrics.

The Maritime Aerosol Network (MAN), as a component of the AERONET network, is an excellent example of the establishment of a global network composed of portable and relatively low-cost sun photometers operating onboard ship platforms with a standardized data processing (Knobelspiesse et al., 2004; Smirnov et al., 2009; Adames et al., 2011). The main goal of MAN is to conduct research on marine aerosols, dust transport, satellite retrieval validation, and atmospheric correction (Adames et al., 2011; Smirnov et al., 2011; Yin et al., 2019) with the hand-held Microtops II sun photometer as the standard instrument. MAN is considered the largest long-term aerosol observation network over the ocean, providing spectral aerosol optical depth (AOD) and precipitable water vapour (PWV) information from the Arctic to Antarctica, inheriting its legacy from the SIMBIOS (Sensor Intercalibration and Merger for Biological and Interdisciplinary Oceanic Studies) NASA program (Fargion et al., 2001; Knobelspiesse et al., 2004). Porter et al. (2001) estimated an average uncertainty in Microtops II AOD ship-based measurements of 0.025 (assuming 2 standard deviations) with calibration error, changes in electronics, filter degradation, temperature effects or poor pointing at the sun (depending on the sea roughness) as the main important contributions to the final error term.

Considering background conditions in remote oceanic regions defined by Smirnov et al. (2002) as AOD at 500 nm below 0.10 (mean value of 0.07), Microtops II is considered a suitable instrument to monitor marine aerosols, extending aerosol characterization to remote marine locations.

Calitoo portable hand-held sun photometer (Djossou et al., 2018; Bayat and Assarenayati, 2023), is a simple, low-cost scientific instrumentation for aerosol remote sensing. It can measure the sun's irradiance at three different wavelengths and directly calculate AOD. This low-cost sun photometer, which costs approximately one order of magnitude less than the Microtops, has been utilized in Western Africa to validate the Warning Advisory System (WAS) for airborne dust (Terradellas et al., 2018; Archer et al., 2024). Additionally, it has been employed on the Global Learning and Observations to Benefit the Environment (GLOBE) student platform, which promotes student science by monitoring environmental parameters using cost-effective equipment (Brooks and Mims, 2001; Butler and MacGregor, 2003; Bayat and Assarenayati, 2023). Some examples of Calitoo AOD measurements can be found in the literature, such as those published

by Léon et al. (2021) and Bayat and Assarenayati (2023), although these are based on short measurement periods or case studies. This inexpensive instrument can be considered a valuable component of a monitoring strategy if it provides sufficient data quality to meet performance targets through extensive evaluation studies and validation with independent reference instrumentation.

This article describes the analysis of the 5-year period (2018–2023) AOD and Ångström Exponent (AE) dataset acquired with the hand-held Calitoo sun photometer by the crew of the *Ángeles Alvariño* research vessel. Commissioned in September 2012 by the crew of the research vessel *Ángeles Alvariño*, from the Spanish Institute of Oceanography (IEO-CSIC) during all its research cruises in this period. The vessel covered a research area approximately from 25° to 50°N and 20°W to 5°E. This extensive geographical area encompasses the Canary Islands, the Portuguese coast, the northern Spanish coast, as well as the western Mediterranean Sea. For it, we have organized this work as follows: in Sections 2 and 3, we give a description of the *Ángeles Alvariño* vessel, study area, the technical description of the instruments and datasets used in this research. Section 4 describes the methodology for AOD calculation and the uncertainty analysis. In Section 5, we present the measurements conducted on the vessel, along with the comparative analysis across various regions using AERONET AOD as reference data for validation, as well as MODIS (Moderate Resolution Imaging Spectroradiometer) and CAMS (Copernicus Atmosphere Monitoring Service) AOD. Finally, a summary and conclusions are provided in Sections 6 and 7, respectively.

2. *Ángeles Alvariño* research vessel

The *Ángeles Alvariño* is an oceanographic vessel (Fig. 1a,b) operated by the Spanish Institute of Oceanography, (IEO; https://www.ieo.es/es/) which is part of the Spanish National Research Council (CSIC) and is dedicated to marine science research. Its focus lies in advancing scientific understanding of the oceans, ensuring the sustainability of fisheries resources, and protecting the marine environment.

This research vessel was launched on 21 February 2012 and commissioned in September 2012. It is one of the most modern research vessels in the Spanish fleet, equipped for various research purposes such as physical and chemical oceanography, marine geology, and fisheries. In recent years, this research vessel has covered a region limited by 25° to 50°N and 20°W to 5°E, participating in different research campaigns in the Canary Islands, the Portuguese coast, the northern Spanish coast, as well as in the western Mediterranean Sea (Fig. 2).

3. Instrumentation and datasets

3.1. Calitoo sun photometer

The Calitoo sun photometer (Fig. 1c) is manufactured by the TENUM company and certified by Laboratoire d'Optique Atmosphérique at Lille (France) (https://www.calitoo.fr/). This device is a portable sun photometer equipped with optical filters that transmit radiation at three specific wavelengths: 465, 540 and 619 nm. Each spectral band contains a photodiode optimized for its respective wavelength range. The Calitoo incorporates a small aperture of less than 2 mm, ensuring that the instrument's recorded light intensity remains unaffected by atmospheric scattering. The precise alignment of the small aperture is achieved using a laser to ensure correct orientation with the optical channels. With dimensions of 210 mm x 100 mm x 35 mm and a weight of 400 grams (with batteries), the photometer is portable and user-friendly. This instrument is utilized for measuring aerosol concentrations in the atmosphere and analyzing their size distribution (Djossou et al., 2018; Bayat and Assarenayati, 2023).

The Calitoo was initially designed for manual operation, although a solar tracker is available. The device includes two openings on one side: the first accommodates sensors for measuring incident solar radiation, and the second guides the operator in aligning the instrument. Sunlight entering through this second aperture is projected onto a small target on the front of the instrument, allowing for easy correction of its position. Moreover, the device display provides real-time readings of the solar intensity of each sensor. Once the operator correctly aligns the instrument, that is, when the real-time readings reach their maximum value, the operator only needs to press a single button on the device. The simplicity of the instrument facilitates its use. Following Léon et al. (2021), the uncertainty of the Calitoo AOD is estimated to be Â±0.02 for all wavelengths, with an expected low calibration drift of 1% yr^{-1} based on post-field measurements. However, a more extensive database will be needed to perform a robust estimation of the uncertainty in Calitoo AOD, along with a comprehensive comparison with independent measurements to verify these results.

The Calitoo observations were collected by the *Ángeles Alvariño* vessel from March 2018 to September 2023 (Fig. 2). Two Calitoos were utilized to collect our dataset. Calitoo #0236 was used in two different periods: from March 30, 2018, to April 11, 2019, and from March 10, 2021, to September 23, 2023, while Calitoo #0405 was used for the remaining period.

Data gaps occurred during ship stops in various Spanish harbours for maintenance, lasting from a few days to several months. Additionally, measurements were exclusively carried out under cloud-free conditions. Operators were instructed to take measurements during periods of unobstructed sunlight. The presence of sub-visible cirrus or fragmented clouds in the field of view introduces fluctuations in atmospheric transmission, as emphasized by Smirnov et al. (2000).

A total of 2829 AOD values were collected using the Calitoo instrument between March 2018 and September 2023 (Fig. 2). Among these, 1483 (52%) were measured in the Canary Islands and along the African coast (region I), 926 (33%) along the Spanish Mediterranean coast (region II), 246 (9%) along the Portuguese coast (region III) and 174 (6%) along the Cantabrian coast and the Bay of Biscay (region IV). Most measurements were taken in the early morning (between 08:00 and 10:00 UTC), comprising 44% of the total, and during the afternoon hours (between 14:00 and 16:00 UTC), accounting for 55%. During the measurement procedure, a minimum of three consecutive measurements were taken within an interval of approximately three minutes to mitigate errors stemming from measurement conditions. Moreover, measurements were conducted under clear-sky conditions.

3.2. AERONET-Cimel sun photometer

The AOD data provided by AERONET–Cimel reference instruments were used for comparison with values derived from Calitoo. The Cimel photometer, as described in Holben et al. (1998), is an automatic sun–sky scanning filter radiometer that measures AOD at 340, 380, 440, 500, 675, 870, and 1020 nm (extended wavelength versions additionally include 1640 nm) with a 1.3° full field of view (FOV) (Holben et al., 1998; Torres et al., 2013). The uncertainty in AOD measurements from Cimel field instruments was estimated to be ±0.01 in the visible (VIS) and near-infrared (IR) ranges, which increased to ±0.02 in the ultraviolet (UV) range (340 and 380 nm) (Eck et al., 1999; Sinyuk et al., 2012).

In this study, we utilized data from three AERONET-Cimel stations located in Santa Cruz de Tenerife in the Canary Islands (28.47°N, 16.25°W, 52 m a.s.l.), El Arenosillo in Huelva (37.10°N, 6.73°W, 59 m a.s.l.) and Palma de Mallorca in the Balearic Islands (39.55°N, 2.62°E, 10 m a.s.l.). Their measurements are compared with the AOD values obtained with Calitoo in three areas: Canary Islands (26°-32°N; 20°-12°W), Huelva (36°-37°N; 6°-8°W) and Balearic Islands (37°-42°N; 0°-5°E). We used AERONET version 3.0 level 2.0 AOD data (Giles et al., 2019) for Santa Cruz de Tenerife for the study period, El Arenosillo until April 2023 and Palma de Mallorca until May 2023, for the rest, the remaining period, level 1.5 data have been utilized.

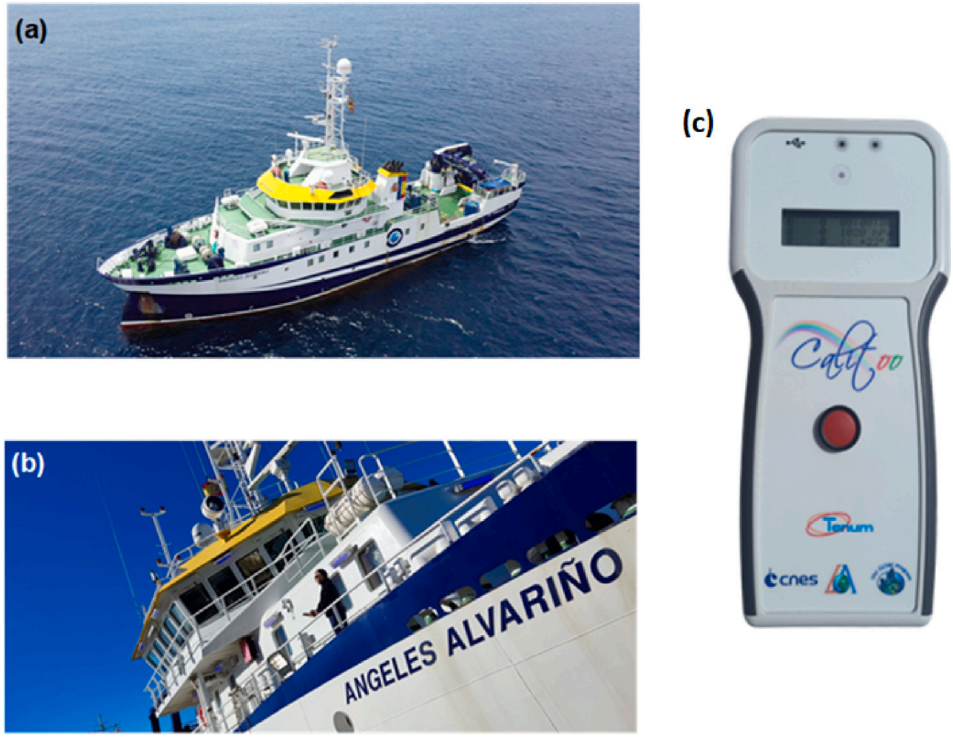

Fig. 1. (a,b) Pictures of the *Ángeles Alvariño* vessel belonging to the Spanish Institute of Oceanography (IEO-CSIC). (c) Calitoo sun photometer.

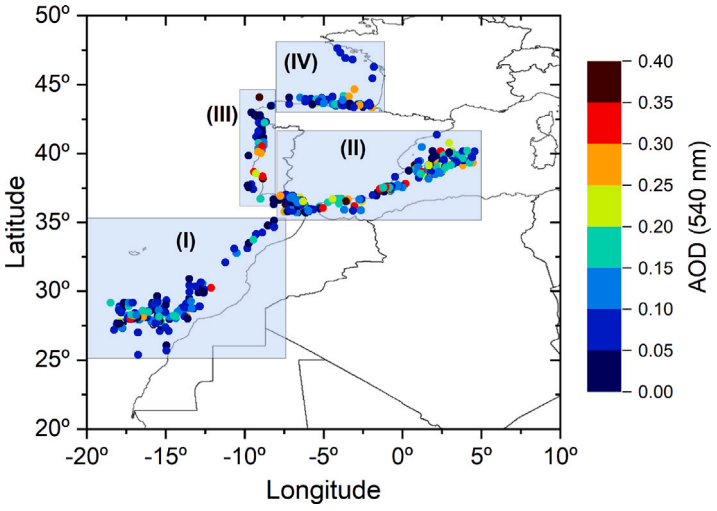

Fig. 2. Map of localization of available Calitoo measurements on board the oceanographic vessel *Ángeles Alvariño* between March 2018 and September 2023. The AOD value at a wavelength of 540 nm is indicated by the color of the dots.

Ship-borne AODs extracted from MAN, component of AERONET, could be an important piece of information in the present study. However, only 19 coincident observations (within a time interval of ±30 min and at a distance of less than 500 km) were accessible for this study. For this reason, MAN data were not included in the comparison or validation study of the Calitoo.

3.3. MODIS aerosol products

The MODIS instrument is aboard the polar-orbiting satellites Terra and Aqua, which belong to the NASA Earth Observing System (EOS). MODIS was launched aboard Terra in 1999 and Aqua in 2002, and allows Earth observation by providing a high level of global coverage and detail. Its radiometer sensitivity enables MODIS to capture information in a broad spectral range. It covers 36 discrete spectral bands ranging from the visible to the thermal infrared (0.62 to 14.365 μm). Moreover, MODIS offers the opportunity to study a diverse array of Earth's surface and atmospheric properties. These spectral channels include visible, near-infrared, and thermal bands, facilitating the retrieval of many parameters such as land surface temperature, vegetation dynamics, cloud properties, and atmospheric composition (Kaufman et al., 1997; Tanré et al., 1997).

In this study, we utilized level 2 products MOD04_3K and MYD04_3K (Collection 6.1; Levy et al., 2015). These products encompass a diverse range of atmospheric variables, including aerosol optical properties. With a spatial resolution of 3 km, this product represents an enhanced version incorporating algorithmic refinements in Dark Target (DT) Aerosol retrieval over urban areas and includes uncertainty estimates for Deep Blue (DB) Aerosol retrievals.

3.4. CAMS reanalysis AOD

Data from the aerosol reanalysis of the Copernicus Atmosphere Monitoring Service (CAMS) provided by the European Centre for Medium-Range Weather Forecasts (ECMWF) (Inness et al., 2013) have been used. This reanalysis is a robust amalgamation of satellite observations assimilated into a comprehensive global model, effectively rectifying model biases on the contrary to observational data (Inness et al., 2013, 2019).

Specifically, our analysis used the ECMWF Atmospheric Composition Reanalysis 4 (EAC4) dataset (Inness et al., 2019). This dataset represents an extensive global atmospheric composition reanalysis product, merging a wide array of remote sensing and ground-level observational data into a continuous, globally available spatiotemporal dataset, all facilitated by a sophisticated numerical atmospheric model (Inness et al., 2019). The dataset boasts high temporal resolution data (at 3-hour intervals) for both total and species-specific AOD measurements. However, it is important to note that the spatial resolution is coarse, at 0.75° × 0.75° across various wavelengths (including 469, 550, 670, 865, and 1240 nm), and our analysis focuses solely on the wavelength of 550 nm.

4. Methodology

4.1. Retrieval of AOD from Calitoo measurements

The AOD was derived from the direct solar radiation measured by Calitoo according to the Beer–Lambert-Bouguer law:

$$V(\lambda) = V_0(\lambda) \cdot e^{-m\tau(\lambda)} \tag{1}$$

where $V(\lambda)$ is the signal measured by the instrument at wavelength (λ), m is the optical air mass, $\tau(\lambda)$ is total the optical depth, and $V_0(\lambda)$ is the instrument calibration constant in the top-of-atmosphere radiation corrected for the Sun-Earth distance.

The calibration constant, $V_0(\lambda)$, has been determined during stops of the *Ángeles Alvariño* at the Santa Cruz de Tenerife harbour (Tenerife, Canary Islands). These stops enabled to exchange/recalibrate the Calitoo instruments, ensuring measurement accuracy over the 5-year period. Calibration of the Calitoo instruments took place at the Izaña high-altitude station (IZO, https://izana.aemet.es/). Calibration procedures were conducted, through an intercomparison analysis of coincident Calitoo and AERONET-Cimel observations at IZO using Eq. (1). It is noteworthy that the limited availability of days (2–3 days) for instrument calibration was due to this port not being the vessel's primary operational base.

The total optical depth, $\tau(\lambda)$, can be expanded by taking into account the contribution of different agents and can be written as:

$$\tau(\lambda) = \tau_R(\lambda) + \tau_a(\lambda) + \tau_{NO_2}(\lambda) + \tau_{H_2O}(\lambda) + \tau_{O_2}(\lambda) + \tau_{O_3}(\lambda) \tag{2}$$

where $\tau_R(\lambda)$ resulting from Rayleigh scattering, which is dependent on station pressure, τ_a denotes the AOD, and the remaining terms account for the absorption by atmospheric gases.

In this study, corrections for Rayleigh scattering have been applied to the three wavelengths, and ozone column corrections have also been implemented at 540 and 619 nm. The remaining terms $\tau_{NO_2}(\lambda)$, $\tau_{H_2O}(\lambda)$ and $\tau_{O_2}(\lambda)$ have been deemed negligible, as confirmed by the transmittances of each gas obtained using the MODerate resolution atmospheric TRANsmission model (MODTRAN; Berk et al., 2000).

Therefore, isolating the AOD in the Beer–Lambert-Bouguer law, it can be calculated as follows:

$$AOD = \frac{1}{m_a} \cdot [lnV_0(\lambda) - lnV(\lambda) - \tau_R \cdot m_R - \tau_{O_3}(\lambda) \cdot m_{O_3}] \tag{3}$$

where:

$$m_a = \frac{1}{cos(\theta) + 0.0548 \cdot (92.65 - \theta)^{-1.452}} \tag{4}$$

$$\tau_R = \frac{P}{P_o} \cdot 0.008569 \cdot \lambda^{-4} \cdot (1 + 0.0113 \cdot \lambda^{-2} + 0.00013 \cdot \lambda^{-4}) \tag{5}$$

$$m_R = \frac{1}{cos(\theta) + 0.50575 \cdot (96.07995 - \theta)^{-1.6364}} \tag{6}$$

$$\tau_{O_3}(\lambda) = u_{O_3} \cdot A_{O_3} \tag{7}$$

$$m_{O_3} = \frac{R + h}{\sqrt{(R + h)^2 - (R + r)^2 \cdot sin^2(\theta)}} \tag{8}$$

In the previous equations, θ represents the solar zenith angle, P denotes the pressure at the measurement site within Earth's atmosphere, P_0 stands for the standard pressure at sea level, λ is the wavelength in micrometers (μm), and u_{O_3} indicates the total ozone column derived from the monthly climatology utilized by AERONET (OMI: Ozone Monitoring Instrument) spanning from 2018 to 2023 (Giles et al., 2019). Two distinct climatologies have been employed to estimate the total column ozone in each region: one for the Canary Islands region (Region I) and another for the Iberian Peninsula regions (Regions II, III, and IV) (see Fig. 2). A_{O_3} denotes the ozone absorption cross-section based on the work of Brion et al. (1993, 1998), R (6370 km) represents the mean radius of Earth, r indicates the station's height above mean sea level in kilometers, and h denotes the mean height of the ozone layer in kilometers (set at 22 km).

Besides, the AOD was calculated at 550 nm to compare the Calitoo measurements with the MODIS and CAMS AOD. For this purpose, we calculated the Ångström Exponent (AE) from the following equation:

$$\tau_a(\lambda) = \beta \cdot \lambda^{(-AE)} \tag{9}$$

where β is the atmospheric turbidity coefficient. AE is calculated with measured AODs ($\tau_a(\lambda_1)$) and ($\tau_a(\lambda_2)$) at two different wavelengths (λ_1 = 465 nm and λ_2 = 619 nm) from the following equation:

$$AE = ln(\tau_a(\lambda_1)/\tau_a(\lambda_2))/ln(\lambda_2/\lambda_1) \tag{10}$$

Therefore, the AOD at 550 nm is calculated as follows:

$$\tau_a(550\ \text{nm}) = \tau_a(540\ \text{nm}) \cdot (0.550/0.540)^{(-AE)} \tag{11}$$

4.2. AOD uncertainty analysis

In the following section, the uncertainty analysis has been addressed for Calitoo AOD retrievals. To do it, the guidelines outlined in the Guide to the Expression of Uncertainty in Measurement (referred to as GUM) were followed. Specifically, the Monte Carlo method (MCM) has been employed as defined in the work by Gum (2008). Calculations were performed using the MetroloPy Python module (accessible at https://pypi.org/project/metrolopy/). The detailed steps can be found in García et al. (2021), but taking into account specific parameters for this work. The number of iterations in each AOD retrieval was set to 10^6, as recommended by the GUM, to achieve a 95% coverage interval.

The MCM has been applied to Eq. (3), in which uncertainties of all variables were obtained from the literature (Table 1), except for V and V_0. For V, its associated uncertainty (ΔV) has been evaluated for each measurement, considering the standard deviation of the recorded counts in consecutive measurements. Pointing errors (dependent on sea roughness), electronic noise and atmospheric variability during measurements are expected to impact on ΔV. Please note that only those consecutive measurements in which there are a minimum of 3

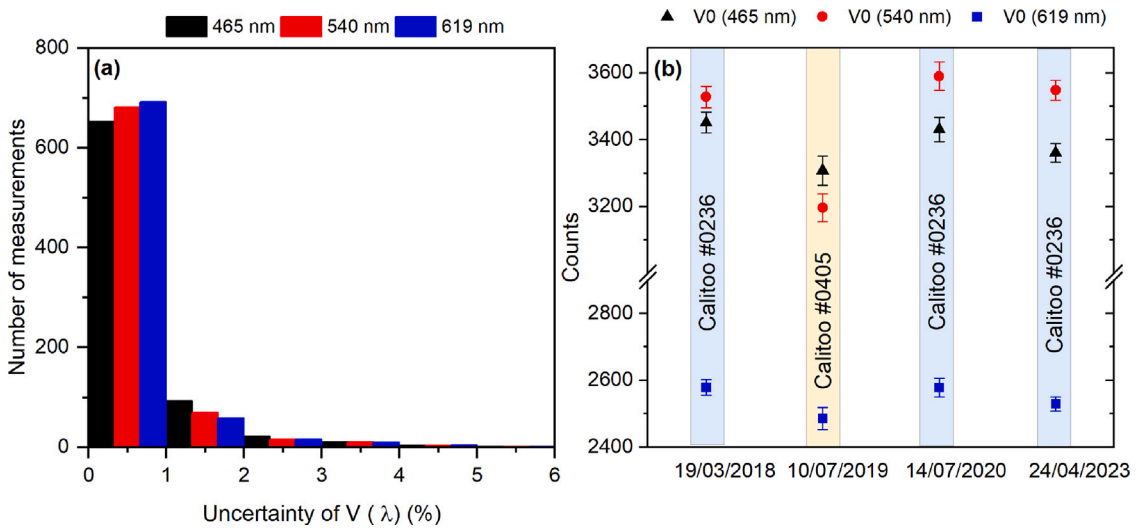

Fig. 3. (a) Frequency distribution of the relative uncertainty of the measurement counts for 465, 540 and 619 nm. (b) Time series of V_0 for three wavelengths. The blue band corresponds with the Calitoo #0236 and the orange one with Calitoo #0405. The error bars correspond to the MCM evaluations.

Table 1
Input parameters uncertainties and their corresponding references. MCM: Monte-Carlo method.

Parameter	Uncertainty	Reference
$V(\lambda)$	5%	–
V_0(465 nm)[a]	±44	MCM
V_0(540 nm)[a]	±43	MCM
V_0(619 nm)[a]	±33	MCM
m_R; m_a; m_{O3}	0.065%	Kasten and Young (1989)
τ_R	0.7%	Fröhlich and Shaw (1980)
u_{O_3}	15%	Huang et al. (2017)
A_{O_3}	0.31%	Tavella et al. (2023)
Sun-Earth distance	0.0001	Spencer et al. (1971)
AOD	±0.01	Holben et al. (1998)

[a] Units: Digital counts.

Table 2
Summary of Calitoo AOD observations. Median, interquartile range (IQR) and number of measurements (N) for AOD between March 2018 and September 2023. Region (I): 25°–35°N, 20°W-0°E, Region (II): 35°–43°N, 7°W-5°E, Region (III): 37°–45°N, 10°–7°W and Region (IV): 43°–47°N, 7°W-0°E.

	Wavelength	AOD Median	IQR	N
Region (I)	**465 nm**	0.090	0.078	
Canary Islands	**540 nm**	0.083	0.076	1483
and African coast	**619 nm**	0.081	0.073	
Region (II)	**465 nm**	0.145	0.149	
Mediterranean Coast	**540 nm**	0.116	0.136	926
	619 nm	0.106	0.118	
Region (III)	**465 nm**	0.112	0.106	
Portuguese coast	**540 nm**	0.084	0.092	246
	619 nm	0.075	0.092	
Region (IV)	**465 nm**	0.111	0.123	
Cantabrian coast	**540 nm**	0.097	0.113	174
and Bay of Vizcaya	**619 nm**	0.085	0.091	

measurements were considered. In addition to that, the time needed to perform the cited measurements should be less than 3 min, as recommended by the manufacturer. The histogram of the uncertainties (in percentage) is shown in Fig. 3(a). A maximum ΔV of 5% is observed, with most of the uncertainties being below 2%. Considering that the Calitoo measurements in this paper were performed by trained (scientific) staff, we have adopted a ΔV value of 5%, representing a conservative assumption that can be considered valid for Calitoo readings performed by non-qualified staff.

Calitoo's calibration, performed at the stops of the vessel, as explained in Section 4.1, is shown in Fig. 3(b). V_0 uncertainty (ΔV_0) was estimated using the same MCM process explained previously. In this case, ΔV_0 values estimated with the MCM are expressed in Table 1 and in the error bars of Fig. 3(b), which are ± 44, ± 43, ± 33 digital counts for 465, 540 and 619 nm, respectively. It must be noted here that, for each channel, only the maximum obtained value in the four available days is included in the MCM evaluation. These values translate to an uncertainty in V_0 < 1.3% for all cases. The time series of V_0 also demonstrates remarkable stability in all wavelengths for Calitoo #0236, mainly considering that nearly 5 years have elapsed between the first and last values of V_0. We found V_0 relative differences in the 5-year period of 2.6% for 465 nm, 1.7% for 540 nm and 1.9% for 619 nm, respectively. This decay rate is similar to that found in Léon et al. (2021).

5. Results

The Calitoo AOD time series between March 2018 and September 2023 is presented in this section (Fig. 4). A total of 2829 handheld-sunphotometer observations were acquired (Table 2; Section 3.1). It should be noted that region I (52%) has the greatest number of measurements while region IV (6%) has the lowest number. The median AOD ranges from a minimum of 0.081 at 619 nm in the region of the Canary Islands and along the African coast (region I), to a maximum of 0.145 at 465 nm on the Mediterranean coast (region II). The highest IQR (interquartile range) can be found in region II, the Mediterranean coast, with a value of 0.149 at 465 nm. In region I, the IQR is remarkably similar in all three wavelengths, whilst more variability is found in the other regions.

The expanded uncertainty (U_{AOD}) of AOD has been incorporated in Fig. 4, determined through the application of the previously cited MCM procedure (see Section 4.2). The black arrows in this figure indicate the calibration dates. The U_{AOD} ranges between 0.008 and 0.050, with a mean of 0.032 ± 0.008 for three wavelengths and no significant drift from the calibration date. For $AOD_{465\ nm}$ <0.05 (11% of the data), the U_{AOD} mean is 0.029 ± 0.009. For $AOD_{465\ nm}$ between 0.05 and 0.20 (66% of the data) the U_{AOD} mean is 0.033 ± 0.008, while for $AOD_{465\ nm}$>0.20 (23% of the data) is 0.036 ± 0.006. The results for 540 and 619 nm spectral bands are similar to those cited for 465 nm, with minor variations. The average uncertainty found for the three spectral bands (0.032 ± 0.008) will be considered the uncertainty associated with Calitoo AOD measurements. This is a conservative estimate that includes measurement and calibration errors as well as errors associated with the aerosol load, air mass, Rayleigh scattering, and gas absorption calculations. Measurement errors (ΔV) such as pointing

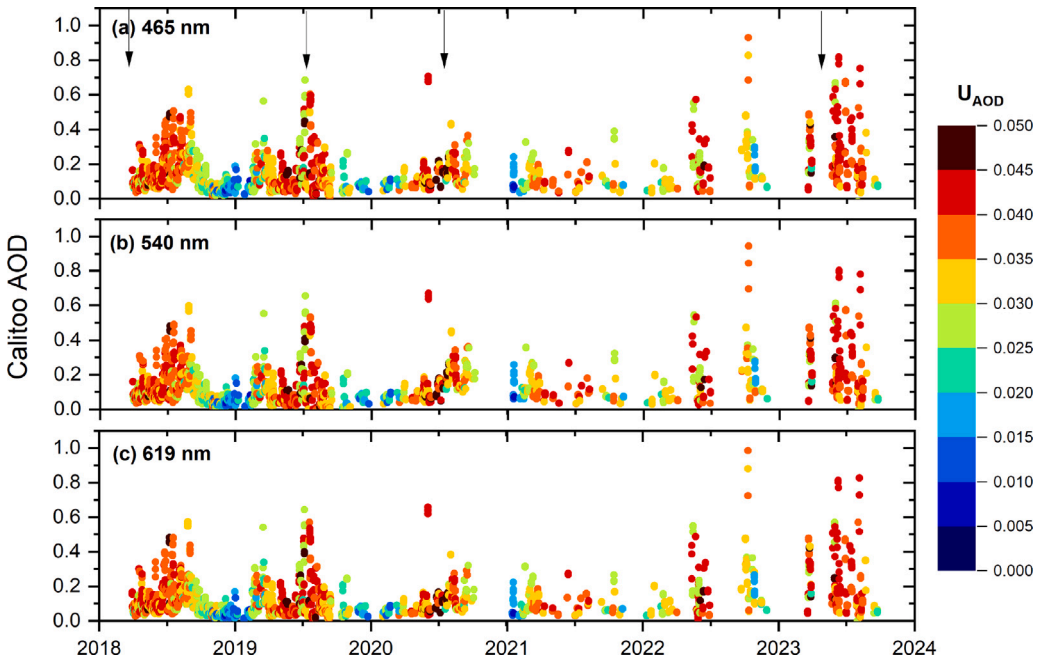

Fig. 4. Times series of Calitoo AOD at (a) 465 nm, (b) 540 nm, and (c) 619 nm measured on board the oceanographic vessel *Ángeles Alvariño* between March 2018 and September 2023. The color scale indicates the expanded uncertainty (U_{AOD}) calculated by means of the Monte Carlo method. The black arrows mark the calibration dates.

errors, electronic noise, or atmospheric variation during measurements are found to dominate the uncertainty analysis.

5.1. Comparison Calitoo-AERONET AOD

In this section, we deal with the comparison between Calitoo AOD and the AOD measured in three AERONET-Cimel stations along the route of the vessel *Ángeles Alvariño*, namely: (1) Santa Cruz de Tenerife (28.47°N, 16.25°W, 52 m a.s.l.), (2) Palma de Mallorca (39.55°N, 2.62°E, 10 m a.s.l.), and (3) El Arenosillo (37.10°N, 6.73°W, 59 m a.s.l.). The Calitoo AOD measurements used in the comparison were filtered to lie in the surroundings of the cited AERONET-Cimel station. Thus, the areas were: (1) 26°-32°N, 20°-12°W (Fig. 5a), (2) 37°-42°N, 0°-5°E (Fig. 5b), and (3) 36°-37°N, 8°-6°W (Fig. 5c), for Santa Cruz de Tenerife, Palma de Mallorca and El Arenosillo stations, respectively. It should be taken into account that the AERONET-Cimel AOD has been determined at 465, 540 and 619 nm, by using Eqs. (9) and (10) for comparison with Calitoo AOD.

The comparison was conducted using coincident measurements within a ±2-minute interval for all wavelengths in both datasets. This methodology yielded an AERONET-Cimel and Calitoo AOD dataset comprising a total of 176 quasi-coincident in-time measurements for the Canary Islands, 49 for the Balearic Islands, and 91 for Huelva. The range of AOD values included in the comparison is broader for the Canary Islands and the Balearic Islands (AOD up to 0.5), while the comparison conducted in Huelva was carried out under AOD conditions restricted to values <0.2. It is important to point out that, for this reason, the data series measured with the Calitoo is not intended to be used in this work to create a climatology of these three study regions, but rather to carry out the necessary validation exercise to demonstrate its viability for aerosol monitoring in different AOD regimes.

Fig. 5 (d,e,f) shows the scatterplots of the AOD data (AERONET-Cimel vs Calitoo) at each Calitoo wavelength. The results reveal a good agreement between Calitoo and AERONET-Cimel AOD (see Table 3), with correlation coefficients (R) of 0.906, 0.879 and 0.836 for 465 nm and 0.917, 0.883, 0.839 for 619 nm in the Canary Islands, Balearic Islands and Huelva, respectively. It may be noted that all correlations show a statistically significant correlation with values of p-value $\ll 0.01$. Root mean square errors (RMSE) and standard deviations (STD) reach their minimum value at 619 nm for the three study regions, with a value of 0.038–0.039 for the Canary and Balearic Islands, and 0.025 for the Huelva area. Generally, for the three wavelengths, the RMSE values are lower for Huelva, since the range of variation in this region is smaller. The negative values of the mean bias (MB; Calitoo AOD – AERONET-Cimel AOD) for the three regions indicate that the values of Calitoo AOD are typically lower than AERONET-Cimel AOD.

AOD differences (Calitoo AOD – AERONET-Cimel AOD) versus the distance in km are shown in Fig. 5(g,h,i). The distance refers to the separation between the point of each measurement on the ship and the location of the AERONET-Cimel station, estimated based on the latitude and longitude of both points. It is observed that there is no dependence between the AOD differences and the distance, although, in the case of Huelva, there are no measurements with a separation of less than approximately 35 km. The farthest measurements from the ground station were made in the Canary Islands, with some measurements taken at a distance of almost 400 km from the coastal AERONET station.

Based on the results presented in Fig. 5 and Table 3, it can be inferred that there is no appreciable impact on the skill scores depending on the wavelength of the Calitoo bands,nor any discernible dependence between stations. The only noticeable variation appears in the MB values in the Balearic Islands, which exhibit significantly higher MB values (up to −0.030). The standard deviation values of AOD differences indicate maximum values of up to 0.043 in the case of the Canary Islands and Huelva, and 0.053 in the Balearic Islands. These values fall within the expected range, considering that AERONET-Cimel uncertainty is ±0.01 in the visible range (Eck et al., 1999) and the maximum uncertainty associated with Calitoo measurements is 0.032 ± 0.008 (see Section 5). The higher RMSE, MB and STD values observed in the Balearic Islands may be due to the limited number of data points used in the comparison, but also to the potential influence of fine-mode aerosols or specific meteorological conditions affecting the AOD variability on short spatial scale, or to the presence of some instrumental bias.

A subsequent investigation on the capabilities of the Calitoo to provide a reliable classification of the type of aerosol has been conducted to help explain the aforementioned differences in AOD. This complementary information is based on the relationship between Calitoo AOD

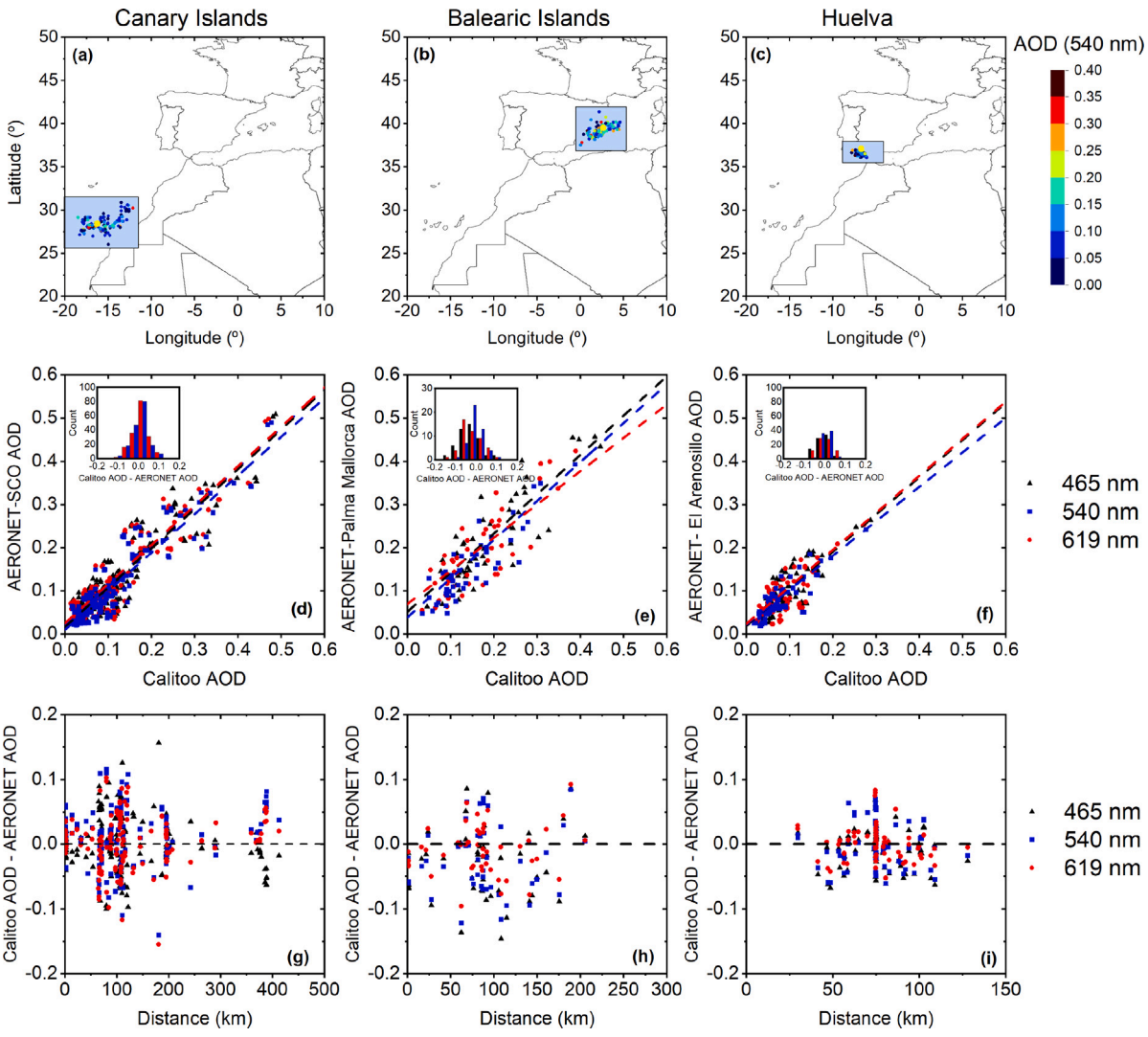

Fig. 5. Map of localization of available Calitoo measurements on board the oceano-graphic vessel *Ángeles Alvariño*: (a) Canary Islands (26°-32°N, 20°-12°W), (b) Balearic Islands (37°-42°N, 0°-5°E), (c) Huelva (36°-37°N, 8°-6°W). The yellow dots indicate the location of the AERONET stations (Santa Cruz de Tenerife, Palma de Mallorca, and El Arenosillo). The AOD value at a wavelength of 540 nm is indicated by the color of the dot. Scatterplot of Calitoo AOD versus AERONET-AOD between March 2018 and September 2023 at 465 nm (black color), 540 nm (blue color), and 619 nm (red color) at (d) Canary Islands, (e) Balearic Islands, (f) Huelva. The dotted lines are the least-squares fits. The small figures represent the occurrence distributions of the AOD differences (Calitoo AOD - AERONET-AOD). Difference between Calitoo AOD and AERONET AOD versus distance in km for (g) Canary Islands, (h) Balearic Islands, and (i) Huelva.

and AE measurements (Holben et al., 2001; Hess et al., 1998; Eck et al., 1999; Smirnov et al., 2002; Basart et al., 2009).

The scatterplots of Calitoo AE (465–619 nm) versus Calitoo $AOD_{540\ nm}$ and AERONET-Cimel AE (440–870 nm) versus AERONET-Cimel $AOD_{540\ nm}$ are presented in Fig. 6. The dataset corresponding to $AOD_{540\ nm} < 0.15$ (for both Calitoo and AERONET-Cimel measurements) has been selected for the study of background conditions (maritime clean) (blue region in Fig. 6), $AOD_{540\ nm} \geq 0.15$ and $AE \leq 0.6$ for dust conditions (orange region), $AOD_{540\ nm} \geq 0.15$ and $0.6 < AE < 1.3$ for mixed conditions (yellow region) and $AOD_{540\ nm} \geq 0.15$ and $AE \geq 1.3$ for polluted conditions (grey region) (Basart et al., 2009). Following this criterion, the predominant conditions in the three study regions are the background conditions with 75% (with a mean and standard deviation AOD of 0.071 ± 0.037), 53% (0.098 ± 0.029) and 93% (0.078 ± 0.029) of the data for the Canary Islands, Balearic Islands and Huelva, respectively. These background conditions refer to clean marine conditions without the influence of anthropogenic (local) aerosols. Dust conditions prevail in the Canary Islands area with 23% of the data (0.269 ± 0.085), compared to 6% and 5% for the Balearic Islands and Huelva, respectively. As reported by Barreto et al. (2022a), the presence of the Saharan Air Layer (SAL) at subtropical latitudes is characterized by a dust-laden layer that strongly affects the Marine Boundary Layer (MBL) that reaches altitudes up to 6 km in summer (Barreto et al., 2022b). According to these authors, the SAL over the Canary Islands can be considered a well-mixed layer with generally fairly constant thermodynamic vertical features and dust particle concentration. These nearly constant aerosol properties persist during its long-range transport due to vertical internal mixing processes (Ryder et al., 2018), explaining the independence of AOD differences with the Calitoo-Cimel distance, at spatial scales of 400 km (Fig. 5). This is a noteworthy finding, as it suggests that Calitoo measurements may be representative of extensive areas in the subtropical region.

Not only dusty conditions, but also clean marine conditions are expected to result in minimal variability of AOD (Smirnov et al., 2002), unlike polluted environments. The Canary Islands and Huelva do not contribute to the pollution events, while measurements taken in the Balearic Islands were affected by pollution in 22% of the cases. Cases of aerosol mixture also turned out to be a high percentage in the Balearic Islands (18%) compared to 2% in the rest of the areas. These findings align well with those reported by Lyamani et al. (2015)

Table 3
Statistics of the Calitoo-AOD and AERONET-AOD comparison performed between March 2018 and September 2023 at Canary Islands (26°–32°N, 20°–12°W), Balearic Islands (37°–42°N, 0°–5°E) and Huelva (36°–37°N, 8°–6°W). N is the number of measurements; RMSE is the root mean square error; MB is the mean bias; STD is the standard deviation. The fit parameters are also included: R (Pearson Correlation coefficient; p-value), slope, and intercept.

	Wavelength	Slope	Intercept	RMSE	MB	STD	R (p-value)
	465 nm	0.903	0.015	0.043	−0.002	0.043	0.906 (≪0.01)
Canary Islands	**540 nm**	0.885	0.016	0.044	−0.003	0.043	0.900 (≪0.01)
(N 176)	**619 nm**	0.907	0.008	0.039	−0.002	0.039	0.917 (≪0.01)
	465 nm	0.997	0.030	0.060	−0.030	0.053	0.879 (≪0.01)
Balearic Islands	**540 nm**	0.919	0.038	0.056	−0.024	0.053	0.838 (≪0.01)
(N 49)	**619 nm**	0.910	0.021	0.038	−0.008	0.038	0.883 (≪0.01)
	465 nm	0.928	0.012	0.030	−0.006	0.030	0.836 (≪0.01)
Huelva	**540 nm**	0.806	0.016	0.033	−0.001	0.030	0.727 (≪0.01)
(N 91)	**619 nm**	0.781	0.015	0.025	−0.001	0.025	0.839 (≪0.01)

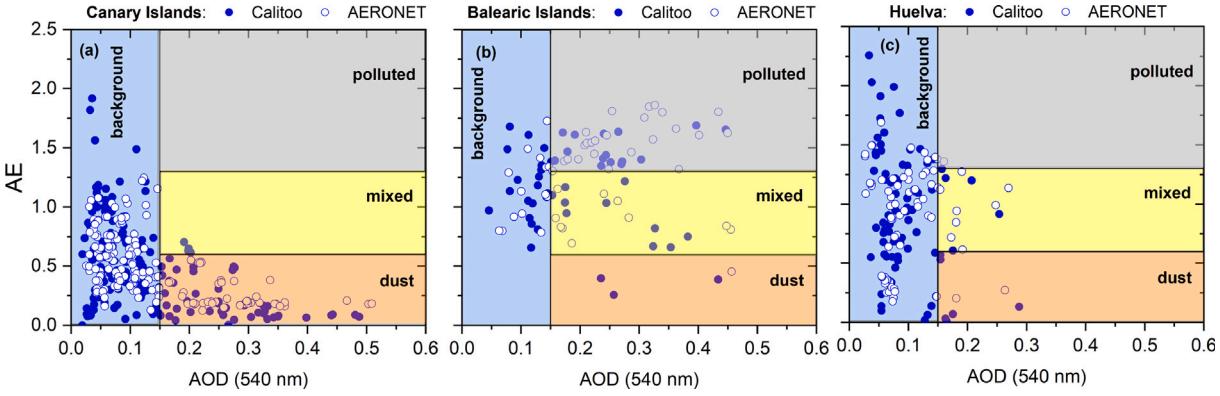

Fig. 6. Scatterplots of the values of Calitoo AE (465–619 nm) versus Calitoo $AOD_{540\ nm}$ (closed circles) and AERONET AE (440–870 nm) versus AERONET $AOD_{540\ nm}$ (open circles) for (a) Canary Islands, (b) Balearic Islands and (c) Huelva. The regions indicate the threshold limits established for background (marine clean) ($AOD_{540\ nm} < 0.15$; blue color), dust ($AOD_{540\ nm} \geq 0.15$ and $AE \leq 0.6$; orange color), mixed ($AOD_{540\ nm} \geq 0.15$ and $0.6 < AE < 1.3$; yellow color) and aerosol polluted conditions ($AOD_{540\ nm} \geq 0.15$ and $AE \geq 1.3$; gray color).

over the western Mediterranean and Rodríguez et al. (2015), Cuevas et al. (2017), Barreto et al. (2022b,a) in the subtropical eastern North Atlantic region.

The predominance of fine mode (polluted or mixed aerosols) in this area with high AOD and AE values is hypothesized to be behind the higher MB and STD observed in Fig. 5 and Table 3.

The same classification performed with AERONET data (Fig. 6, shown with open dots) yields similar results, except for polluted conditions in the Balearic Islands. In this case, maximum differences of 21% were observed (22% in Calitoo measurements, compared to 43% in AERONET-Cimel measurements). Differences below 10% were observed for the remaining aerosol regimes and stations, suggesting that variability in fine-mode AOD is likely the cause of the differences observed in Figs. 5 and 6, as well as in Table 3.

5.2. Comparison MODIS and CAMS AOD versus Calitoo data

The Calitoo AOD at 550 nm was compared with the AOD data at 550 nm retrieved from the operational MODIS AOD product at a 3-km resolution (MOD04_3K) and the CAMS EAC4 reanalysis datasets, for the period spanning from 2018 to 2023 (Fig. 7). Comparisons were made by aligning measurements from both databases within a ±30-minute window. For MODIS data, measurements within a 5 × 5 pixel square around the satellite overpass were considered, as outlined in previous studies (Ichoku et al., 2002; Léon et al., 2021). The CAMS reanalysis has a spatial resolution of 0.75°x0.75° and a temporal resolution of 3 h (Inness et al., 2013, 2019). For the MODIS database, 237 matches with the Calitoo measurements along the coast of Spain were found (Fig. 7a), and 1113 matches were found for CAMS (Fig. 7b).

The correlation and statistical metrics for the comparison between MODIS and CAMS AOD with Calitoo AOD are presented in Table 4, considering four regions (labeled I to IV). The slope closest to one is found in region IV for Calitoo vs. CAMS, with a value of 1.024, while the worst is in region III for Calitoo vs. MODIS at 0.529. Notably, the best slope for Calitoo vs. MODIS is 0.711 (region IV), and the worst for Calitoo vs. CAMS is 0.614 (region III).

The comparison between Calitoo and MODIS generally shows worse skill scores than the comparison between Calitoo and CAMS (Table 4). Nevertheless, it should be noted that the number of available coincident measurements is quite different for CAMS and MODIS, mainly due to the higher temporal frequency of the CAMS reanalysis, as outlined at the beginning of this section. In the case of the Calitoo-MODIS comparison,Â the slopes (0.53–0.71) are lower than those reported by Gupta et al. (2018) for the Europe-Mediterranean region (1.06) in the 2000–2015 period. However, correlation coefficients (0.69–0.87) and RMSE values (0.09–0.15) are similar to those found by these authors (0.79 and 0.11, respectively). A MB (Calitoo-MODIS) of −0.063 was found for the four regions, pointing to a general overestimation of MODIS AOD in agreement with the values found by Gupta et al. (2018) by comparing with AERONET-Cimel in the Europe-Mediterranean region.

Low intercept and RMSE values were found in the Calitoo-CAMS comparison in all regions (Table 4), with the exception of region IV (0.081 and 0.197, respectively), which is attributed to the low number of AOD pairs in this region. RMSE values range between 0.053 and 0.063, which are consistent with the results retrieved by Kapsomenakis et al. (2022) along a 19-year study period (2003–2021) using all the available AERONET observations over the Northern Africa, the Middle East and Southern Europe (NAMEE) region. Correlation coefficients (R) for regions I and II (0.84–0.85) are also in agreement with the results published by Kapsomenakis et al. (2022) and Langerock et al. (2024) in the NAMEE region. MB values (Calitoo-CAMS) of −0.034, −0.026 and −0.013 (not shown in Table 4) were found in regions I,

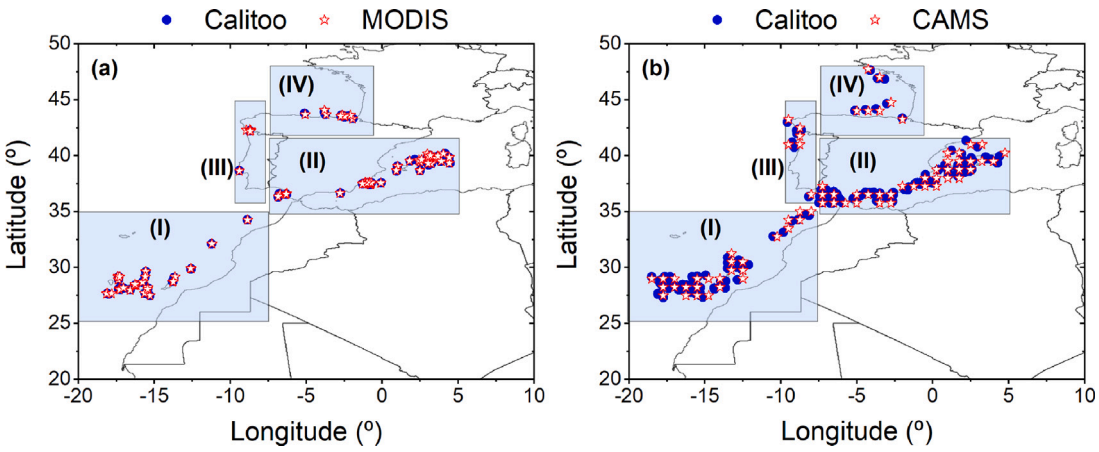

Fig. 7. Map of available Calitoo measurements on board the ocean-graphic vessel *Ángeles Alvariño* coinciding with (a) MODIS AOD and (b) CAMS AOD measurements between March 2018 and September 2023.

Table 4
AOD comparison statistics for Calitoo with MODIS and CAMS between March 2018 and September 2023. The regions represent (I) the Canary Islands and the African coast, (II) the Mediterranean coast, (III) the Portuguese coast and (IV) the Cantabrian coast and Bay of Vizcaya. The statistical parameters are defined in Table 3 and n.s. indicates that the p-value is not significant.

	Calitoo AOD-MODIS AOD					Calitoo AOD-CAMS AOD				
Region	Slope	Intercept	RMSE	R (p-value)	N	Slope	Intercept	RMSE	R (p-value)	N
(I)	0.681	−0.004	0.094	0.864 (≪0.01)	78	0.801	−0.007	0.053	0.849 (≪0.01)	314
(II)	0.585	0.035	0.151	0.693 (≪0.01)	129	0.807	0.004	0.063	0.838 (≪0.01)	636
(III)	0.529	0.049	0.106	0.872 (≪0.01)	14	0.614	0.021	0.055	0.686 (≪0.01)	65
(IV)	0.711	0.048	0.123	0.423 (n.s.)	16	1.024	0.081	0.197	0.269 (n.s.)	29
Total	**0.614**	**0.024**	**0.130**	**0.732 (≪0.01)**	**237**	**0.786**	**0.006**	**0.066**	**0.783 (≪0.01)**	**1113**

II and III (average of −0.024), pointing to a general overestimation of CAMS AOD in the three regions. These values are in agreement with the annual MB (AERONET-CAMS) between −0.03 and 0.01 in the Mediterranean region found by Kapsomenakis et al. (2022) but not with the AOD underestimation over the subtropical North Atlantic and the Sahel belt expected for CAMS (Kapsomenakis et al., 2022; Langerock et al., 2024). A more extensive comparison database would be necessary to conduct a more accurate comparison.

6. Summary

In this paper, we present a 5-year assessment of AOD and AE data acquired from the hand-held Calitoo sun photometer onboard the oceanographic vessel *Ángeles Alvariño*. The Calitoo device quantifies solar irradiance at three specific wavelengths (465, 540, and 619 nm). The observational period extends from March 2018 to September 2023, encompassing a total of 2829 measurements. This extensive dataset provides AOD and AE information for various regions, including the Canary Islands and the African coast (region I: 52% of the data), the Mediterranean coast (region II: 33%), Portuguese coast (region III: 9%), Cantabrian coast and Bay of Biscay (region IV) with 6% of the data. Data gaps occurred during ship stops for maintenance. The median AOD of this dataset ranged from 0.081 at 619 nm in region I to 0.145 at 465 nm in region II. The IQR was highest in region II at 465 nm (0.149) and lowest in region I at 619 nm (0.073).

A Monte Carlo method was employed to estimate the uncertainty in the Calitoo AOD, resulting in an expanded uncertainty (U_{AOD}) ranging from 0.008 to 0.050, with a mean value of 0.032 ± 0.008 for the three wavelengths.

AERONET-Cimel AODs were used as reference information in a validation analysis of the Calitoo AOD values in the Canary Islands, Huelva, and Balearic Islands. In particular, three AERONET stations were used in this validation analysis: Santa Cruz de Tenerife, El Arenosillo (Huelva), and Palma de Mallorca. The comparison showed a good agreement, with correlation coefficients ranging from 0.727 to 0.917 for the three wavelengths at the three stations. RMSE was lowest at 619 nm for three study regions, with a value of 0.038–0.039 for the Canary and Balearic Islands, and 0.025 for the Huelva area. Calitoo AOD values were generally lower than those of AERONET-Cimel (MB ranging between −0.030 and −0.001), within the combined uncertainties expected for Cimel and Calitoo. Calitoo AOD and AE information have also proven reliable for classifying aerosol types, which could significantly improve our understanding of aerosols in remote or under-monitored areas.

A subsequent AOD comparison analysis between Calitoo-MODIS and Calitoo-CAMS shows negative mean bias of −0.063 and −0.024, respectively. These values indicate a general overestimation by MODIS and CAMS in the study regions. However, a more extensive comparison database is needed to draw more precise conclusions about the effects of diverse aerosols and their climatology on the satellite products.

7. Conclusions

The study provides a comprehensive evaluation of the Calitoo hand-held sun-photometer's performance in measuring AOD, using AERONET-Cimel information as the reference. A subsequent comparison analysis compared its data with established satellite (MODIS) and atmospheric composition reanalysis (CAMS) products. The key conclusions are as follows:

- Calitoo has demonstrated remarkable calibration stability over the 5-year period covered in this study (<0.26%), with an estimated AOD uncertainty of 0.032 ± 0.008. This is a significant finding, as low-cost sensors are often prone to sensor-to-sensor variability and rapid decay rates, complicating their use as effective components in monitoring networks.
- Calitoo measurements show strong agreement with AERONET-Cimel data. Small AOD underestimation (between −0.030 and

−0.001) and high correlations (>0.73) are the main results obtained in the AOD validation conducted under different aerosol regimes.
- Our results confirm that Calitoo measurements are representative over large spatial scales in the subtropical region, particularly under marine clean and dusty conditions.
- A reliable aerosol-type classification has been conducted using Calitoo AOD and AE data, which could significantly enhance our understanding of aerosols in key areas.
- The methodology and data series presented in this study can serve as a foundation for future Calitoo deployments and validation/assimilation plans for satellite and modeling products, as well as its potential integration with other observational platforms. Given the low cost of the Calitoo, it can be deployed onboard a large number of merchant and passenger ships or in remote and under-monitored land areas, providing near real-time AOD/AE data for comprehensive aerosol studies. This helps to fill significant gaps in existing global atmospheric composition monitoring networks, thereby enhancing the robustness of aerosol monitoring efforts.

CRediT authorship contribution statement

Rosa D. García: Writing – review & editing, Writing – original draft, Validation, Supervision, Software, Methodology, Conceptualization. **África Barreto:** Writing – review & editing, Writing – original draft, Supervision, Methodology, Investigation. **Celia Rey:** Writing – original draft, Software, Data curation. **Eugenio Fraile-Nuez:** Writing – original draft, Resources. **Alba González-Vega:** Writing – original draft, Resources. **Sergio F. León-Luis:** Writing – original draft, Methodology, Conceptualization. **Antonio Alcantara:** Writing – original draft, Methodology, Conceptualization. **A. Fernando Almansa:** Writing – original draft, Methodology, Conceptualization. **Carmen Guirado-Fuentes:** Writing – original draft. **Pablo González-Sicilia:** Writing – original draft, Methodology, Conceptualization. **Victoria E. Cachorro:** Writing – original draft. **Frederic Bouchar:** Writing – original draft.

Declaration of competing interest

The authors declare the following financial interests/personal relationships which may be considered as potential competing interests: Africa Barreto reports administrative support was provided by Spanish State Meteorological Agency Izaña Atmospheric Research Center. Africa Barreto reports a relationship with Spanish State Meteorological Agency Izaña Atmospheric Research Center that includes: employment. If there are other authors, they declare that they have no known competing financial interests or personal relationships that could have appeared to influence the work reported in this paper.

Acknowledgments

This work is part of the activities of the WMO-Measurement Lead Centre for aerosols and water vapor remote sensing instruments (MLC). The authors would like to thank Dr. Emilio Cuevas for his support and leadership in this project, making the necessary institutional collaboration possible to carry out the measurements presented in this paper. We also would like to thank the crew and the technician team of R/V *Ángeles Alvariño*, particularly Jorge López Sixto, for the collection of the Calitoo sample. We gratefully acknowledge the data provided by the AERONET network (El Arenosillo Station: Margarita Yela González; Palma de Mallorca: Jose Maria San Atanasio and Ana Díaz Rodríguez). The AERONET sun photometers at the Izañ'/a Observatory (IZO) were calibrated through the AEROSPAIN Central Facility (https://aerospain.aemet.es/), supported by the European Community Research Infrastructure Action under the ACTRIS grant (agreement no. 871115). The authors thank all the principal investigators and their staff for establishing and maintaining the NASA-MODIS and ECMWF-CAMS.

Data availability

The AERONET-Cimel data from Santa Cruz de Tenerife, Palma de Mallorca, and El Arenosillo are available on the AERONET website: https://aeronet.gsfc.nasa.gov/. MODIS products are available from the Goddard Space Flight Center Level 1 and the Atmosphere Archive and Distribution System ((https://ladsweb.nascom.nasa.gov)). The CAMS global reanalysis (EAC4) is available in: https://ads.atmosphere.copernicus.eu/. The Calitoo data are available upon request to the corresponding authors.

References

Adames, A.F., Reynolds, M., Smirnov, A., Covert, D.S., Ackerman, T.P., 2011. Comparison of moderate resolution imaging spectroradiometer ocean aerosol retrievals with ship-based sun photometer measurements from the around the americas expedition. J. Geophys. Res.: Atmos. 116 (D16), http://dx.doi.org/10.1029/2010JD015440, arXiv:https://agupubs.onlinelibrary.wiley.com/doi/pdf/10.1029/2010JD015440, URL https://agupubs.onlinelibrary.wiley.com/doi/abs/10.1029/2010JD015440.

Archer, J.-M., Barreto, Á., Bi, J., Biggs, R., Castell, N., deSouza, P., Dye, T., Fujita, R., Giordano, M.R., Gonzalez, M.E., Hasenkopf, C., Hassani, A., Hodoli, C.G., Hofman, J., Nicolás Jorge Huneeus, R.J., Kroll, J., Labrador, L., Leghrib, R., Levy, R.C., Marques, T., Martins, L.D., McMahon, E., Mead, M.I., Molina, L.T., Montgomery, A., Morawska, L., Ning, Z., Peltier, R., Popoola, O., Rojas, N., Retama, A., Schneider, P., Shairsingh, K., Strużewska, J., Tang, B., Poppel, M.V., Westervelt, D.M., Zhang, Y., Zheng, M., 2024. Integrating low-cost sensor systems and networks to enhance air quality applications. In: Chair, Publications Board World Meteorological Organization (WMO),Geneva, Switzerland (Ed.), WMO/GAW Report No. 263. Geneva, URL https://library.wmo.int/viewer/68924/download?file=GAW-293_report_en.pdf&type=pdf&navigator=1.

Barreto, Á., Cuevas, E., García, R.D., Carrillo, J., Prospero, J.M., Ilić, L., Basart, S., Berjón, A.J., Marrero, C.L., Hernández, Y., Bustos, J.J., Ničković, S., Yela, M., 2022a. Long-term characterisation of the vertical structure of the saharan air layer over the canary islands using lidar and radiosonde profiles: implications for radiative and cloud processes over the subtropical atlantic ocean. Atmos. Chem. Phys. 22 (2), 739–763. http://dx.doi.org/10.5194/acp-22-739-2022, URL https://acp.copernicus.org/articles/22/739/2022/.

Barreto, A., García, R., Guirado-Fuentes, C., Cuevas, E., Almansa, A., Milford, C., Toledano, C., Expósito, F., Díaz, J.P., León-Luis, S.F., 2022b. Aerosol characterisation in the subtropical eastern north atlantic region using long-term AERONET measurements. Atmos. Chem. Phys. 22 (17), 11105–11124. http://dx.doi.org/10.5194/acp-22-11105-2022, URL https://acp.copernicus.org/articles/22/11105/2022/.

Basart, S., Pérez, C., Cuevas, E., Baldasano, J.M., Gobbi, G.P., 2009. Aerosol characterization in northern africa, northeastern atlantic, mediterranean basin and middle east from direct-sun AERONET observations. Atmos. Chem. Phys. 9, 8265–8282. http://dx.doi.org/10.5194/acp-9-8265-2009.

Bayat, A., Assarenayati, A., 2023. How to measure the amount of aerosol optical thickness in the atmosphere in a simple way: A calitoo handheld sun-photometer measurement. Atmos. Environ. 295, 119570. http://dx.doi.org/10.1016/j.atmosenv.2022.119570, URL https://www.sciencedirect.com/science/article/pii/S1352231022006355.

Berk, A., Acharya, P.K., Anderson, G., Chetwynd, J.H., Hoke, M.L., 2000. Reformulation of the MODTRAN band model for higher spectral resolution. In: Proceedings Spue the International Society for Opitcal Engineering. International Society for Optical Engineering; 1999, pp. 190–198.

Brion, J., Chakir, A., Charbonnier, J., Daumont, D., Parisse, C., Malicet, J., 1998. Absorption spectra measurements for the ozone molecule in the 350–830 nm region. J. Atmospher. Chem. 30 (2), 291–299.

Brion, J., Chakir, A., Daumont, D., Malicet, J., Parisse, C., 1993. High-resolution laboratory absorption cross section of O3. Temperature effect. Chem. Phys. Lett. 213 (5–6), 610–612.

Brooks, D.R., Mims, III, F.M., 2001. Development of an inexpensive handheld LED-based sun photometer for the GLOBE program. J. Geophys. Res.: Atmos. 106 (D5), 4733–4740. http://dx.doi.org/10.1029/2000JD900545, arXiv:https://agupubs.onlinelibrary.wiley.com/doi/pdf/10.1029/2000JD900545, URL https://agupubs.onlinelibrary.wiley.com/doi/abs/10.1029/2000JD900545.

Butler, D., MacGregor, I., 2003. Globe: Science and education. J. Geosci. Educ. 51, 9–20. http://dx.doi.org/10.5408/1089-9995-51.1.9.

Cuevas, E., Gómez-Peláez, A.J., Rodríguez, S., Terradellas, E., Basart, S., García, R.D., E., G.O., Alonso-Pérez, S., 2017. The pulsating nature of large-scale saharan dust transport as a result of interplays between mid-latitude rossby waves and the north african dipole intensity. Atmos. Environ. 167, 586–602. http://dx.doi.org/10.1016/j.atmosenv.2017.08.059, URL https://www.sciencedirect.com/science/article/pii/S1352231017305757.

Cuevas, E., Romero-Campos, P.M., Kouremeti, N., Kazadzis, S., Räisänen, P., García, R.D., Barreto, A., Guirado-Fuentes, C., Ramos, R., Toledano, C., Almansa, F., Gröbner, J., 2019. Aerosol optical depth comparison between GAW-PFR and AERONET-cimel radiometers from long-term (2005–2015) 1 min synchronous measurements. Atmos. Meas. Tech. 12 (8), 4309–4337. http://dx.doi.org/10.5194/amt-12-4309-2019, URL https://www.atmos-meas-tech.net/12/4309/2019/.

Djossou, J., Léon, J.-F., Akpo, A.B., Liousse, C., Yoboué, V., Bedou, M., Bodjrenou, M., Chiron, C., Galy-Lacaux, C., Gardrat, E., Abbey, M., Keita, S., Bahino, J., Touré N'Datchoh, E., Ossohou, M., Awanou, C.N., 2018. Mass concentration, optical depth and carbon composition of particulate matter in the major southern west african cities of cotonou (benin) and abidjan (côte d'ivoire). Atmos. Chem. Phys. 18 (9), 6275–6291. http://dx.doi.org/10.5194/acp-18-6275-2018, URL https://acp.copernicus.org/articles/18/6275/2018/.

Eck, T., Holben, B., Reid, J., Dubovik, O., Smirnov, A., O'neill, N., Slutsker, I., Kinne, S., 1999. Wavelength dependence of the optical depth of biomass burning, urban, and desert dust aerosols. J. Geophys. Res.: Atmos. 104 (D24), 31333–31349. http://dx.doi.org/10.1029/1999JD900923.

Fargion, G., Barnes, R., Mcclain, C., 2001. In situ aerosol optical thickness collected by the SIMBIOS program (1997–2000): Protocols, and and data QC and analysis.

Forster, P., Storelvmo, T., Armour, K., Collins, W., Dufresne, J.-L., Frame, D., Lunt, D., Mauritsen, T., Palmer, M., Watanabe, M., Wild, M., Zhang, H., 2021. The earth's energy budget, climate feedbacks, and climate sensitivity. In: Masson-Delmotte, V., Zhai, P., Pirani, A., Connors, S., Péan, C., Berger, S., Caud, N., Chen, Y., Goldfarb, L., Gomis, M., Huang, M., Leitzell, K., Lonnoy, E., Matthews, J., Maycock, T., Waterfield, T., Yelekçi, O., Yu, R., Zhou, B. (Eds.), Climate Change 2021: The Physical Science Basis. Contribution of Working Group I To the Sixth Assessment Report of the Intergovernmental Panel on Climate Change. Cambridge University Press, Cambridge, United Kingdom and New York, NY, USA, pp. 923–1054. http://dx.doi.org/10.1017/9781009157896.009.

Fröhlich, C., Shaw, G.E., 1980. New determination of Rayleigh scattering in the terrestrial atmosphere. Appl. Opt. 19 (11), 1773–1775. http://dx.doi.org/10.1364/AO.19.001773.

García, R.D., Cuevas, E., Cachorro, V.E., García, O.E., Barreto, Á., Almansa, A.F., Romero-Campos, P.M., Ramos, R., Pó, M., Hoogendijk, K., Gross, J., 2021. Water vapor retrievals from spectral direct irradiance measured with an EKO MS-711 spectroradiometer—Intercomparison with other techniques. Remote Sens. 13 (3), 350. http://dx.doi.org/10.3390/rs13030350.

Garnés-Morales, G., Montávez, J.P., Halifa-Marín, A., Jiménez-Guerrero, P., 2023. Role of aerosols on atmospheric circulation in regional climate experiments over europe. Atmosphere 14 (3), 491. http://dx.doi.org/10.3390/atmos14030491, URL https://www.mdpi.com/2073-4433/14/3/491, Number: 3 Publisher: Multidisciplinary Digital Publishing Institute.

Giles, D.M., Sinyuk, A., Sorokin, M.G., Schafer, J.S., Smirnov, A., Slutsker, I., Eck, T.F., Holben, B.N., Lewis, J.R., Campbell, J.R., Welton, E.J., Korkin, S.V., Lyapustin, A.I., 2019. Advancements in the aerosol robotic network (AERONET) version 3 database – automated near-real-time quality control algorithm with improved cloud screening for sun photometer aerosol optical depth (AOD) measurements. Atmos. Meas. Tech. 12 (1), 169–209. http://dx.doi.org/10.5194/amt-12-169-2019, URL https://amt.copernicus.org/articles/12/169/2019/.

Giordano, M.R., Malings, C., Pandis, S.N., Presto, A.A., McNeill, V., Westervelt, D.M., Beekmann, M., Subramanian, R., 2021. From low-cost sensors to high-quality data: A summary of challenges and best practices for effectively calibrating low-cost particulate matter mass sensors. J. Aerosol Sci. 158, 105833. http://dx.doi.org/10.1016/j.jaerosci.2021.105833, URL https://www.sciencedirect.com/science/article/pii/S0021850221005644.

Gum, I., 2008. Guide to the Expression of Uncertainty in Measurement,(1995) with Supplement 1, Evaluation of measurement data, JCGM 101: 2008. Organization for Standardization, article.

Gupta, P., Remer, L.A., Levy, R.C., Mattoo, S., 2018. Validation of MODIS 3 km land aerosol optical depth from NASA's EOS terra and aqua missions. Atmos. Meas. Tech. 11 (5), 3145–3159. http://dx.doi.org/10.5194/amt-11-3145-2018, URL https://amt.copernicus.org/articles/11/3145/2018/.

Hess, M., Koepke, P., Schult, I., 1998. Optical properties of aerosols and clouds: The software package OPAC. Bull. Am. Meteorol. Soc. 79 (5), 831–844. http://dx.doi.org/10.1175/1520-0477(1998)079<0831:OPOAAC>2.0.CO;2, URL https://journals.ametsoc.org/view/journals/bams/79/5/1520-0477_1998_079_0831_opoaac_2_0_co_2.xml.

Holben, B., Eck, T., Slutsker, I., Tanré, D., Buis, J., Setzer, A., Vermote, E., Reagan, J., Kaufman, Y., Nakajima, T., Lavenu, F., Jankowiak, I., Smirnov, A., 1998. AERONET—A federated instrument network and data archive for aerosol characterization. Remote Sens. Environ. 66 (1), 1–16. http://dx.doi.org/10.1016/S0034-4257(98)00031-5.

Holben, B., Tanré, D., Smirnov, A., Eck, T.F., Slutsker, I., Abuhassan, N., Newcomb, W.W., Schafer, J.S., Chatenet, B., Lavenu, F., Kaufman, Y.J., Castle, J.V., Setzer, A., Markham, B., Clark, D., Frouin, R., Halthore, R., Karneli, A., O'Neill, N.T., Pietras, C., Pinker, R.T., Voss, K., Zibordi, G., 2001. An emerging ground-based aerosol climatology: Aerosol optical depth from AERONET. J. Geophys. Res.: Atmos. 106 (D11), 12067–12097. http://dx.doi.org/10.1029/2001JD900014, arXiv:https://agupubs.onlinelibrary.wiley.com/doi/pdf/10.1029/2001JD900014, URL https://agupubs.onlinelibrary.wiley.com/doi/abs/10.1029/2001JD900014.

Huang, G., Liu, X., Chance, K., Yang, K., Bhartia, P.K., Cai, Z., Allaart, M., Ancellet, G., Calpini, B., Coetzee, G.J.R., Cuevas-Agulló, E., Cupeiro, M., De Backer, H., Dubey, M.K., Fuelberg, H.E., Fujiwara, M., Godin-Beekmann, S., Hall, T.J., Johnson, B., Joseph, E., Kivi, R., Kois, B., Komala, N., König-Langlo, G., Laneve, G., Leblanc, T., Marchand, M., Minschwaner, K.R., Morris, G., Newchurch, M.J., Ogino, S.-Y., Ohkawara, N., Piters, A.J.M., Posny, F., Querel, R., Scheele, R., Schmidlin, F.J., Schnell, R.C., Schrems, O., Selkirk, H., Shiotani, M., Skrivánková, P., Stübi, R., Taha, G., Tarasick, D.W., Thompson, A.M., Thouret, V., Tully, M.B., Van Malderen, R., Vömel, H., von der Gathen, P., Witte, J.C., Yela, M., 2017. Validation of 10-year SAO OMI ozone profile (PROFOZ) product using ozonesonde observations. Atmos. Meas. Tech. 10 (7), 2455–2475. http://dx.doi.org/10.5194/amt-10-2455-2017, URL https://amt.copernicus.org/articles/10/2455/2017/.

Ichoku, C., Chu, D.A., Mattoo, S., Kaufman, Y.J., Remer, L.A., Tanré, D., Slutsker, I., Holben, B.N., 2002. A spatio-temporal approach for global validation and analysis of modis aerosol products. Geophys. Res. Lett. 29 (12), MOD1–1–MOD1–4. http://dx.doi.org/10.1029/2001GL013206.

Inness, A., Ades, M., Agustí-Panareda, A., Barré, J., Benedictow, A., Blechschmidt, A.-M., Dominguez, J.J., Engelen, R., Eskes, H., Flemming, J., Huijnen, V., Jones, L., Kipling, Z., Massart, S., Parrington, M., Peuch, V.-H., Razinger, M., Remy, S., Schulz, M., Suttie, M., 2019. The CAMS reanalysis of atmospheric composition. Atmos. Chem. Phys. 19 (6), 3515–3556. http://dx.doi.org/10.5194/acp-19-3515-2019, URL https://acp.copernicus.org/articles/19/3515/2019/.

Inness, A., Baier, F., Benedetti, A., Bouarar, I., Chabrillat, S., Clark, H., Clerbaux, C., Coheur, P., Engelen, R.J., Errera, Q., Flemming, J., George, M., Granier, C., Hadji-Lazaro, J., Huijnen, V., Hurtmans, D., Jones, L., Kaiser, J.W., Kapsomenakis, J., Lefever, K., Leitão, J., Razinger, M., Richter, A., Schultz, M.G., Simmons, A.J., Suttie, M., Stein, O., Thépaut, J.-N., Thouret, V., Vrekoussis, M., Zerefos, C., the MACC team, 2013. The MACC reanalysis: an 8 yr data set of atmospheric composition. Atmos. Chem. Phys. 13 (8), 4073–4109. http://dx.doi.org/10.5194/acp-13-4073-2013, URL https://acp.copernicus.org/articles/13/4073/2013/.

Kapsomenakis, J., Zerefos, C., Langerock, B., Errera, Q., Basart, S., Cuevas, E., Bennouna, Y., Thouret, V., Arola, A., Pitkänen, M., Blechschmidt, A.-M., Richter, A., Eskes, H., Tsikerdekis, T., Benedictow, A., Schulz, M., Bouarar, I., Warneke, T., 2022. Validation report for the CAMS global reanalyses of aerosols and reactive trace gases, years 2003 - 2021. http://dx.doi.org/10.24380/g18s-zdi, URL https://atmosphere.copernicus.eu/sites/default/files/publications/CAMS2_82_2022SC1_D82.4.2.1-2022_reanalysis_validation.pdf.

Kasten, F., Young, A.T., 1989. Revised optical air mass tables and approximation formula. Appl. Opt. 28 (22), 4735–4738. http://dx.doi.org/10.1364/AO.28.004735.

Kaufman, Y., Tanré, D., Remer, L.A., Vermote, E., Chu, A., Holben, B., 1997. Operational remote sensing of tropospheric aerosol over land from eos moderate resolution imaging spectroradiometer. J. Geophys. Res.: Atmos. 102 (D14), 17051–17067. http://dx.doi.org/10.1029/96JD03988.

Knobelspiesse, K.D., Pietras, C., Fargion, G.S., Wang, M., Frouin, R., Miller, M.A., Subramaniam, A., Balch, W.M., 2004. Maritime aerosol optical thickness measured by handheld sun photometers. Remote Sens. Environ. 93 (1), 87–106. http://dx.doi.org/10.1016/j.rse.2004.06.018, URL https://www.sciencedirect.com/science/article/pii/S0034425704002056.

Kobayashi, H., Shiobara, M., 2015. Development of new shipborne aureolemeter to measure the intensities of direct and scattered solar radiation on rolling and pitching vessel. In: Remote Sensing of Clouds and the Atmosphere XX, Vol. 9640. SPIE, pp. 270–278.

Langerock, B., Arola, A., Benedictow, A., Bennouna, Y., Blake, L., Bouarar, I., Cuevas, E., Errera, Q., Eskes, H., Griesfeller, J., Ilic, L., Kapsomenakis, J., Mortier, A., Pison, I., Pitkänen, M., Richter, A., Schoenhardt, A., Schulz, M., Thouret, V., Tsikerdekis, A., Warneke, T., Zerefos, C., 2024. Validation report of the CAMS global reanalysis of aerosols and reactive trace gases, years 2003–2023. http://dx.doi.org/10.24380/G8H7-KD21, URL https://atmosphere.copernicus.eu/node/1140.

Léon, J.-F., Akpo, A.B., Bedou, M., Djossou, J., Bodjrenou, M., Yoboué, V., Liousse, C., 2021. $PM_{2.5}$ surface concentrations in southern west african urban areas based on sun photometer and satellite observations. Atmos. Chem. Phys. 21 (3), 1815–1834. http://dx.doi.org/10.5194/acp-21-1815-2021, URL https://acp.copernicus.org/articles/21/1815/2021/.

Levy, R., Hsu, C., et al., 2015. MODIS atmosphere L2 aerosol product. NASA MODIS adaptive processing system. Goddard Space Flight Center, USA, http://dx.doi.org/10.5067/MODIS/MOD04_L2.061.

Li, J., Carlson, B.E., Yung, Y.L., Lv, D., Hansen, J., Penner, J.E., Liao, H., Ramaswamy, V., Kahn, R.A., Zhang, P., Dubovik, O., Ding, A., Lacis, A.A., Zhang, L., Dong, Y., 2022. Scattering and absorbing aerosols in the climate system. Nat. Rev. Earth Environ. 3 (6), 363–379. http://dx.doi.org/10.1038/s43017-022-00296-7, URL https://www.nature.com/articles/s43017-022-00296-7.

Li, Z., Zhao, X., Kahn, R., Mishchenko, M., Remer, L., Lee, K.-H., Wang, M., Laszlo, I., Nakajima, T., Maring, H., 2009. Uncertainties in satellite remote sensing of aerosols and impact on monitoring its long-term trend: a review and perspective. Annal. Geophys. 27 (7), 2755–2770. http://dx.doi.org/10.5194/angeo-27-2755-2009, URL https://angeo.copernicus.org/articles/27/2755/2009/.

Lyamani, H., Valenzuela, A., Perez-Ramirez, D., Toledano, C., Granados-Muñoz, M.J., Olmo, F.J., Alados-Arboledas, L., 2015. Aerosol properties over the western mediterranean basin: temporal and spatial variability. Atmos. Chem. Phys. 15

(5), 2473–2486. http://dx.doi.org/10.5194/acp-15-2473-2015, URL https://acp.copernicus.org/articles/15/2473/2015/.

Nakajima, T., Campanelli, M., Che, H., Estellés, V., Irie, H., Kim, S.-W., Kim, J., Liu, D., Nishizawa, T., Pandithurai, G., et al., 2020. An overview of and issues with sky radiometer technology and SKYNET. Atmos. Meas. Tech. 13 (8), 4195–4218.

Peltier, R., Castell, N., Clements, A., Dye, T., Hueglin, C., Kroll, J., Shih-Chun, Lung, C., Ning, Z., Parsons, M., Penza, M., Reisen, F., von Schneidemesser, E., Arfire, A., Boso, À., Fu, Q., Hagan, D., Henshaw, G., Jayaratne, R., Zellweger, C., 2021. An update on low-cost sensors for the measurement of atmospheric composition. Technical Report GAW Report No. 1215, World Meteorological Organization, WMO, Geneva, Switzerland.

Persad, G., Samset, B.H., Wilcox, L.J., Allen, R.J., Bollasina, M.A., Booth, B.B.B., Bonfils, C., Crocker, T., Joshi, M., Lund, M.T., Marvel, K., Merikanto, J., Nordling, K., Undorf, S., van Vuuren, D.P., Westervelt, D.M., Zhao, A., 2023. Rapidly evolving aerosol emissions are a dangerous omission from near-term climate risk assessments. Environ. Res. Climate 2 (3), 032001. http://dx.doi.org/10.1088/2752-5295/acd6af.

Rodríguez, S., Cuevas, E., Prospero, J.M., Alastuey, A., Querol, X., López-Solano, J., García, M.I., Alonso-Pérez, S., 2015. Modulation of saharan dust export by the north african dipole. Atmos. Chem. Phys. 15 (13), 7471–7486. http://dx.doi.org/10.5194/acp-15-7471-2015, URL https://acp.copernicus.org/articles/15/7471/2015/.

Ryder, C.L., Marenco, F., Brooke, J.K., Estelles, V., Cotton, R., Formenti, P., McQuaid, J.B., Price, H.C., Liu, D., Ausset, P., Rosenberg, P.D., Taylor, J.W., Choularton, T., Bower, K., Coe, H., Gallagher, M., Crosier, J., Lloyd, G., Highwood, E.J., Murray, B.J., 2018. Coarse-mode mineral dust size distributions, composition and optical properties from AER-D aircraft measurements over the tropical eastern atlantic. Atmos. Chem. Phys. 18 (23), 17225–17257. http://dx.doi.org/10.5194/acp-18-17225-2018, URL https://acp.copernicus.org/articles/18/17225/2018/.

Sinyuk, A., Holben, B.N., Smirnov, A., Eck, T.F., Slutsker, I., Schafer, J.S., Giles, D.M., Sorokin, M., 2012. Assessment of error in aerosol optical depth measured by AERONET due to aerosol forward scattering. Geophys. Res. Lett. 39 (23), http://dx.doi.org/10.1029/2012GL053894.

Smirnov, A., Holben, B., Eck, T., Dubovik, O., Slutsker, I., 2000. Cloud-screening and quality control algorithms for the aeronet database. Remote Sens. Environ. 73 (3), 337–349. http://dx.doi.org/10.1016/S0034-4257(00)00109-7.

Smirnov, A., Holben, B.N., Giles, D.M., Slutsker, I., O'Neill, N.T., Eck, T.F., Macke, A., Croot, P., Courcoux, Y., Sakerin, S.M., Smyth, T.J., Zielinski, T., Zibordi, G., Goes, J.I., Harvey, M.J., Quinn, P.K., Nelson, N.B., Radionov, V.F., Duarte, C.M., Losno, R., Sciare, J., Voss, K.J., Kinne, S., Nalli, N.R., Joseph, E., Krishna Moorthy, K., Covert, D.S., Gulev, S.K., Milinevsky, G., Larouche, P., Belanger, S., Horne, E., Chin, M., Remer, L.A., Kahn, R.A., Reid, J.S., Schulz, M., Heald, C.L., Zhang, J., Lapina, K., Kleidman, R.G., Griesfeller, J., Gaitley, B.J., Tan, Q., Diehl, T.L., 2011. Maritime aerosol network as a component of AERONET – first results and comparison with global aerosol models and satellite retrievals. Atmos. Meas. Tech. 4 (3), 583–597. http://dx.doi.org/10.5194/amt-4-583-2011, URL https://amt.copernicus.org/articles/4/583/2011/.

Smirnov, A., Holben, B.N., Kaufman, Y.J., Dubovik, O., Eck, T.F., Slutsker, I., Pietras, C., Halthore, R.N., 2002. Optical properties of atmospheric aerosol in maritime environments. J. Atmos. Sci. 59 (3), 501–523. http://dx.doi.org/10.1175/1520-0469(2002)059<0501:OPOAAI>2.0.CO;2, URL https://journals.ametsoc.org/view/journals/atsc/59/3/1520-0469_2002_059_0501_opoaai_2.0.co_2.xml.

Smirnov, A., Holben, B.N., Slutsker, I., Giles, D.M., McClain, C.R., Eck, T.F., Sakerin, S.M., Macke, A., Croot, P., Zibordi, G., Quinn, P.K., Sciare, J., Kinne, S., Harvey, M., Smyth, T.J., Piketh, S., Zielinski, T., Proshutinsky, A., Goes, J.I., Nelson, N.B., Larouche, P., Radionov, V.F., Goloub, P., Krishna Moorthy, K., Matarrese, R., Robertson, E.J., Jourdin, F., 2009. Maritime aerosol network as a component of aerosol robotic network. J. Geophys. Res.: Atmos. 114 (D6), http://dx.doi.org/10.1029/2008JD011257, arXiv:https://agupubs.onlinelibrary.wiley.com/doi/pdf/10.1029/2008JD011257, URL https://agupubs.onlinelibrary.wiley.com/doi/abs/10.1029/2008JD011257.

Spencer, R.P., Lange, R.C., Treves, S., 1971. Use of 135mBa and 131Ba as bone-scanning agents. J. Nucl. Med. 12 (5), 216–221.

Tanré, D., Kaufman, Y., Herman, M., Mattoo, S., 1997. Remote sensing of aerosol properties over oceans using the MODIS/EOS spectral radiances. J. Geophys. Res.: Atmos. 102 (D14), 16971–16988. http://dx.doi.org/10.1029/96JD03437.

Tavella, P., Gressier, V., Wielgosz, R., Stock, M., Milton, M., 2023. News from the BIPM laboratories—2022. Metrologia 60 (2), 025006. http://dx.doi.org/10.1088/1681-7575/acb776.

Terradellas, E., Werner, E., Basart, S., Benincasa, F., 2018. Warning Advisory System for Sand and Dust Storm in Burkina Faso. Technical Report SDS-WAS Report No. SDS-WAS-2018-001, WMO SDS-WAS, Barcelona, Spain.

Toledo, F., Garrido, C., Díaz, M., Rondanelli, R., Jorquera, S., Valdivieso, P., 2018. AOT retrieval procedure for distributed measurements with low-cost sun photometers. J. Geophys. Res.: Atmos. 123 (2), 1113–1131. http://dx.doi.org/10.1002/2017JD027309, arXiv:https://agupubs.onlinelibrary.wiley.com/doi/pdf/10.1002/2017JD027309, URL https://agupubs.onlinelibrary.wiley.com/doi/abs/10.1002/2017JD027309.

Torres, B., Dubovik, O., Fuertes, D., Schuster, G., Cachorro, V.E., Lapyonok, T., Goloub, P., Blarel, L., Barreto, A., Mallet, M., Toledano, C., Tanré, D., 2017. Advanced characterisation of aerosol size properties from measurements of spectral optical depth using the GRASP algorithm. Atmos. Meas. Tech. 10 (10), 3743–3781. http://dx.doi.org/10.5194/amt-10-3743-2017, URL https://amt.copernicus.org/articles/10/3743/2017/.

Torres, B., Toledano, C., Berjón, A., Fuertes, D., Molina, V., Gonzalez, R., Canini, M., Cachorro, V.E., Goloub, P., Podvin, T., Blarel, L., Dubovik, O., Bennouna, Y., de Frutos, A.M., 2013. Measurements on pointing error and field of view of cimel-318 sun photometers in the scope of AERONET. Atmos. Meas. Tech. 6 (8), 2207–2220. http://dx.doi.org/10.5194/amt-6-2207-2013, URL https://amt.copernicus.org/articles/6/2207/2013/.

Wehrli, C., 2000. Calibrations of filter radiometer for determination of atmospheric optical depth. Metrologia 37, 419. http://dx.doi.org/10.1088/0026-1394/37/5/16.

Wehrli, C., 2005. GAW–PFR: A network of aerosol optical depth observations with precision filter radiometers. In: WMO/GAW Experts Workshop on a Global Surface Based Network for Long Term Observations of Column Aerosol Optical Properties, Tech. Rep., GAW Report. (162).

Yin, Z., Ansmann, A., Baars, H., Seifert, P., Engelmann, R., Radenz, M., Jimenez, C., Herzog, A., Ohneiser, K., Hanbuch, K., Blarel, L., Goloub, P., Dubois, G., Victori, S., Maupin, F., 2019. Aerosol measurements with a shipborne sun–sky–lunar photometer and collocated multiwavelength Raman polarization lidar over the Atlantic ocean. Atmos. Meas. Tech. 12 (10), 5685–5698. http://dx.doi.org/10.5194/amt-12-5685-2019, URL https://amt.copernicus.org/articles/12/5685/2019/.